

ESR STUDY OF  $\text{AlCl}_3$  GRAPHITE INTERCALATED COMPOUNDS

R.M. Stein

Instituto de Instrumentação, Centro Técnológico para Informática  
 (CTI) Caixa Postal 6162, 13081, Campinas, São Paulo, Brazil.

L.Walmsley, S.Rolla and C.Rettori

Instituto de Física, Universidade Estadual de Campinas UNICAMP  
 Caixa Postal, 1165, 13081, Campinas, São Paulo, Brazil.

## INTRODUCTION

Conduction Carrier spin resonance (CCSR) is an excellent tool for the study of graphite intercalation compounds (1) (GICs) and highly oriented pyrolytic graphite (HOPG) (2). Drastic changes in the resonance parameters have been reported when HOPG is intercalated with either donor alkali-metal atoms (3,4) or acceptor halide molecules (5,6). Thus the study of these effects can give valuable contribution to a better understanding of the transport properties, band structure, phase transition, etc., in these highly anisotropic materials.

In this work we report CCSR experiments in the acceptor  $\text{AlCl}_3$ -GICs, stage 2,4 and 7 from low ( $\approx 10\text{K}$ ) to room temperatures.

We show that for thin samples of  $\text{AlCl}_3$ -GICs the temperature dependence of the in-plane  $\rho_a(T)$  and the c-axis  $\rho_c(T)$  resistivities, can be obtained from the temperature dependence of the intensity and lineshape of the CCSR. The results indicate that the main contribution to  $\rho_a$  and  $\rho_c$  comes from the electron phonon scattering and thermally activated hopping mechanisms respectively.

In a recent report (7), experiments in  $\text{AlCl}_3$ -GICs stage 7, revealed a striking phase transition at  $T_c=170\text{K}$ . We have attributed this to a quasi-two-dimensional (2D) "order-disorder" first order phase transition experienced by the intercalant  $\text{AlCl}_3$  molecules. The observation of a well defined hysteresis cycle in the resonance parameters (line-width, intensity and diffusion time) induced us to admit the existence of a metastable phase below the transition temperature.

## EXPERIMENTS

Single stage n=2, 4 and 7 samples of  $\text{AlCl}_3$ -GICs were prepared using a conventional two zone vapor growth technique (8). Quartz tube of 4 mm inner diameter and 0,5 mm wall appropriated for the CCSR experiments were used for sample preparation. The stage of the samples were determined by X-ray in a conventional  $\theta - 2\theta$  scan. CCSR experiments were carried out in a conventional Varian E-15 X-band reflection spectrometer. Samples of  $7 \times 3 \times 0,1 \text{ mm}^3$  were placed inside the cavity such that the microwave magnetic field ( $H_1$ ) remained always perpendicular to the c-axis. This guarantees that for thin samples the wave penetrates mainly along the c-axis direction and therefore the skin depth will be governed by  $\rho_a$ . The external magnetic field was perpendicular to the c-axis to prevent magnetic field frequency modulation effects on the lineshape (9).

## RESULTS

All samples showed a single "metallic" resonance with an asymmetry parameter A/B ratio greater than 2.55 which can be analysed in terms of Dyson's theory (10) for the limit of thick samples, i.e. when the skin depth is much smaller than the thickness of the sample (11).

Figure 1 shows the experimental temperature dependence of the square of the relative intensity and diffusion time obtained from the resonances of the stage 2 and 4 samples. Within the experimental accuracy no temperature and stage dependence was observed in

the g-value ( $g=2.0035 \pm 0.0006$ ). Small increase of the linewidth, from about 4 to 5 Gauss, toward low temperature was observed.

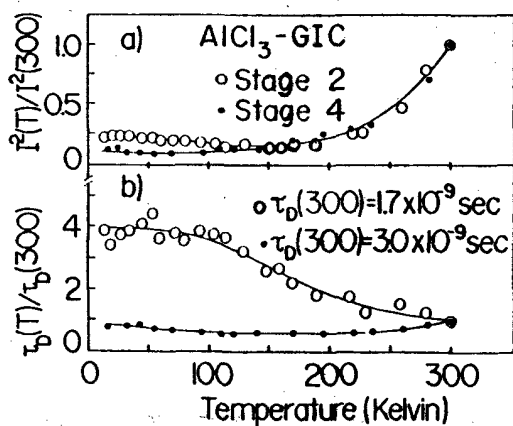


Fig.1. CCSR parameters in  $\text{AlCl}_3$ -GICs stage 2 and 4, (a) square of the relative intensity and (b) diffusion time.

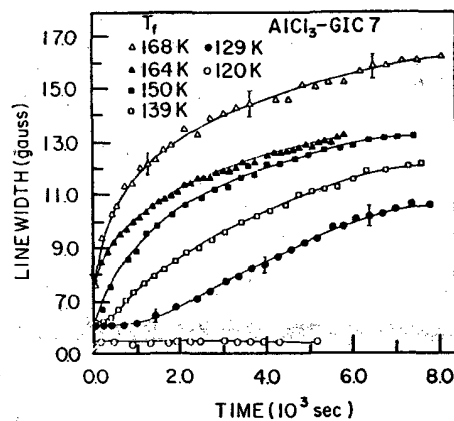


Fig.2. Time dependence of the CCSR linewidth in the stage 7  $\text{AlCl}_3$ -GIC at various temperature below the critical temperature  $T_c=170\text{K}$

Figure 2 shows for stage 7, the time dependence of the CCSR linewidth for various temperatures  $T_f$  between 120K and 170K. After a quenching of approximately 400K/min. from room to low temperature ( $T \approx 100\text{K}$ ), the temperature was quickly raised up to a final value  $T_f$  ( $120\text{K} < T_f < 170\text{K}$ ), where the time evolution of the resonance was monitored during approximately two hours.

In order to emphasize the different kinetics observed when this temperature is reached after cooling or heating the sample, we show in fig.3 the time broadening of the linewidth at  $T_f=160\text{K}$  when the temperature  $T_f$  is approached from the high temperature side and from the low temperature side of the transition. From these results it is evident that the system is "memorizing" its previous thermal history, suggesting a first-order character for this order-disorder phase transformation.

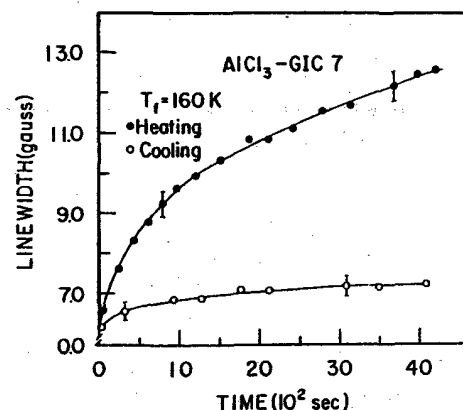


Fig.3 Time dependence of the CCSR linewidth in the stage 7  $\text{AlCl}_3$ -GIC at  $T_f=160\text{K}$ . Open circles correspond to data taken when the temperature  $T_f$  was obtained by quenching from the room temperature, and closed circles correspond to data taken when the temperature  $T_f$  was obtained by heating from a low temperature  $T \approx 100\text{K}$ , which was previously obtained by quenching from room temperature.

#### ANALYSIS AND DISCUSSION

All our  $\text{AlCl}_3$ -GICs show, at room temperature, a single isotropic resonance and an intensity approximately five times larger than that corresponding to a comparable sample size of HOPC. We can therefore argue that the observed resonance comes mainly from a system of unpaired spins associated to the conduction carriers (holes in our case) created during the intercalation process.

Figure 1a shows the temperature dependence of the square of the relative resonance intensity for stage 2 and 4 samples. As we mentioned above, the experimental results indicate that the thickness of the samples were always much larger than the skin depth. Therefore, the intensity of the resonance will be proportional to the skin depth and, consequently, the square of the resonance intensity should scale with the in-plane resistivity. For GICs the carrier's density of states at the Fermi level can be taken to be temperature independent. Thus the temperature dependence of  $\rho_a$  will be determined by the temperature dependence of the square of the relative resonance intensity only

$$\rho_a(T)/\rho_a(300) = I^2(T)/I^2(300) \quad (1)$$

The experimental points in figure 1a actually follow the typical temperature dependence of  $\rho_a$  usually measured in acceptor GICs (12,13), and also predicted theoretically by Pietronero and Strassler (14) for the scattering of the conduction carriers by both the phonons of the graphite layers and the modes of the charged intercalating molecules. The shape of the observed resonances in all our experiments are typically Dysonian-like with an asymmetry parameter, A/B ratio, larger than the diffusionless limit A/B=2.55. According to Dyson's theory (10) this indicates that the resonance spins are diffusing across a skin depth which is smaller than the thickness of the sample. For this limit and using the analysis given by Feher and Kip (11) we can obtain the diffusion time from the lineshape of the resonance.

As we mentioned above for the geometry adopted in our experiments, the skin depth is governed by  $\rho_a$ , then, according to Khanna (5) the diffusion time will be determined by  $\rho_a$  and  $\rho_c$ :

$$\tau_D(T) = \{N(E_F)e^2c^2/2\pi\omega\}\rho_a(T)\rho_c(T) \quad (2)$$

where  $N(E_F)$  is the carrier's density of states at the Fermi level and  $\omega$  the microwave frequency.

For GICs the density of states at the Fermi level can be considered temperature independent (15). Therefore, the temperature dependence of the diffusion time will be mainly determined by  $\rho_a(T)$  and  $\rho_c(T)$ . Figure 1b shows the temperature dependence of the diffusion time for the stage 2 and 4 samples. The evaluation of the diffusion time already includes the small temperature dependence of the linewidth.

It is interesting to note that from eq. 2  $\rho_c(T)$  can be determined from  $\tau_D(T)$  and  $\rho_a(T)$  which are obtained from the lineshape and intensity of the resonance, respectively i.e.

$$\begin{aligned} \frac{\rho_c(T)}{\rho_c(300)} &= \frac{\tau_D(T)/\tau_D(300)}{\rho_a(T)/\rho_a(300)} \\ &= \frac{\tau_D(T)/\tau_D(300)}{I^2(T)/I^2(300)} \end{aligned} \quad (3)$$

Figure 4 shows  $\rho_c(T)$  obtained for stage 2 and 4. At high temperature this results suggest a thermally activated process for the c-axis conductivity, probably a hopping-like mechanism

$$\rho_h = \rho_{oh} \exp \{E/KT\}$$

and at low temperature a metallic-like behaviour with a stage dependent residual resistivity, which might have its origin in narrow highly conducting channels (16) existing along the c-axis.

$$\rho_m = \rho_{om} + \beta T^n$$

We found that  $\rho_c(T)$  shown in figure 4, can be closely reproduced by this phenomenological approach with a set of parameters

$$\begin{aligned} \rho_{om}/\rho_{oh} &= (800 \pm 100), \quad \beta/\rho_{oh} = 6 \\ n=1, \quad E &= (1250 \pm 50)K \text{ for stage 2} \end{aligned}$$

and

$$\rho_{\text{om}}/\rho_{\text{oh}} = (45 \pm 5), \beta/\rho_{\text{oh}} = 0.5$$

$$n=1, E = (560 \pm 20) \text{ K} \text{ for stage 4}$$

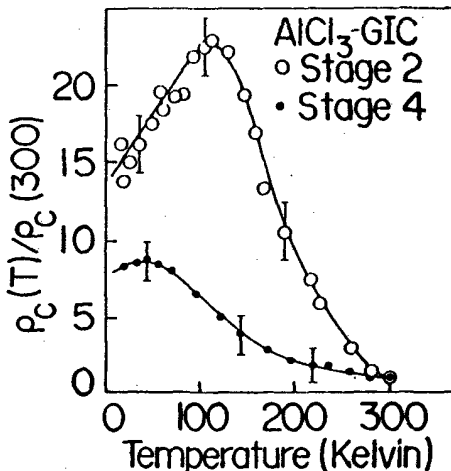


Fig. 4 Temperature dependence of the relative c-axis resistivity.

Figure 5 shows that for temperatures just below  $T_c$  the time broadening of the linewidth shows a scaling behaviour

$$\{\Delta H(t) - \Delta H(0)\} \propto t^n \quad (4)$$

The best fit of the experimental data at 164K and 168K gives  $n=0.42 \pm 0.06$ .

According to Elliot's theory (17) the main contribution to the CCSR linewidth is given by the spin lattice relaxation through phonon scattering via conduction carrier spin-orbit coupling. Elliot's calculation leads to a linewidth which is proportional to the inverse of the conduction carrier's mean free path ( $\Delta H \alpha \lambda^{-1}$ ). In our previous work (7,9) we attributed the observed hysteresis cycle in the CCSR linewidth to an order-disorder first-order phase transition, experienced by the  $\text{AlCl}_3$  molecules in the intercalant layers, which in turn affects the in-plane conduction carrier mobility.

Recent in-plane diffuse x-ray scattering experiments in  $\text{SbCl}_5$ -GICs by Homma and Clarke (18) revealed that one of the coexisting intercalated molecular species,  $\text{SbCl}_3$ , experiences an order-disorder phase transition at  $T_c=230\text{K}$ . They

identified the low temperature solid-like phase as an almost commensurate (2% off)  $(\sqrt{39} \times \sqrt{39}) \text{ R} (\pm 16.1^\circ)$  superlattice. Ultrasonic experiments (19) and ac calorimetry (20) in  $\text{SbCl}_5$ -GICs, have also attributed the observed transition at 230K to a disorder-liquid to incommensurated-solid phase experienced by the intercalant  $\text{SbCl}_3$  molecular species.

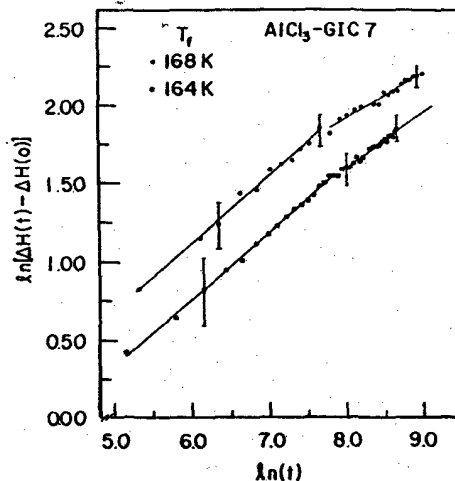


Fig.5 - Time evolution of the CCSR linewidth in the stage 7  $\text{AlCl}_3$ -GIC at 164K (squares) and 168K (circles). The solid lines are fits to scaling behavior (see text).

Following these ideas we suggest that in our stage 7  $\text{AlCl}_3$ -GIC, upon cooling through the first-order phase transition at  $T_c=170\text{K}$  the supercooled-liquid-like phase may freeze in many small domains or islands of a weakly incommensurate structure of  $\text{AlCl}_3$  molecules. If the linear sizes of the domains are much smaller than  $(1 + \Delta l)(1 + \Delta l)/\Delta l = l^2/\Delta l$  (19,21), which corresponds to a characteristic domain with the molecules occupying all the positions between the bottom and the top of the graphite potential, most of the intercalant molecules will be registered near the bottom of the graphite potential wells, yielding an almost unperturbed potential on the graphite layers and consequently an almost unchanged CCSR linewidth at the transition. Now, when the temperature is raised we claim that near  $T_c$  but

before that the superheated-solid-to-liquidlike phase transformation takes place, the intercalant molecules may have enough thermal energy to migrate and the domains grow in time. When their size becomes comparable to  $1^2/\Delta l$  most of the molecules will be shifted from the bottom of the graphite potential wells. This will probably modify the charge density distribution on the carbon layers, which in turn may shorten the conduction carrier mean free path, leading to the observed time broadening of the linewidth. Alternatively, it is possible that the growth of these microdomains may allow the formation of regions, within the Daumas-Herold domains (14), with higher aluminium to carbon concentration which, via spin-orbit coupling (17), causes the shortening of the conduction carriers mean free path, leading in turn, to the observed time broadening of the CCSR linewidth. In both cases the CCSR linewidth would be directly measuring the time growing of the average linear domains size ( $L$ ),

$$\{\Delta H(t) - \Delta H(0)\} \propto \lambda^{-1} \propto L \quad (5)$$

This is supported by the observed power-law evolution of the experimental time broadening of the linewidth shown in figure 5.

Monte Carlo simulations, performed by Sahni et al (21) of the kinetics of domain growth in 2D systems quenched from high temperature ( $T > T_c$ ) to low temperature ( $0.5T_c < T < T_c$ ), for both small and large  $Q$  degeneracies, show an universal or lattice-independent power-law behavior for all values of  $Q$  but with exponents falling gradually from the classical value  $1/2$  ( $Q=2$  Ising limit) predicted by Lifshitz (22) and Allen and Cahn (23) for antiphase domain coarsening to a constant value of  $0.41$  for large  $Q$  ( $Q > 30$ ). Since no simulations of incommensurate structure have been done yet, our thermal broadening of the linewidth near  $T_c$  agrees, in terms of scaling, only qualitatively with Monte Carlo simulations for either triangular square, or even honeycomb lattices

with large  $Q$  values. At temperatures below  $T_c$ , however, our results show that the kinetics becomes slower, and at even lower temperatures ( $T < 140K$ ) the domain configuration seems to be initially frozen (see fig.2). Although Monte Carlo simulations (21) for square or honeycomb lattices show strong pinning effects at low temperatures, and although Lifshitz (22) and Safran (24) have discussed the difficulty in equilibrating systems with high degeneracy, we cannot associate one of these structures with our low-temperature phase. First, as we said before, there are no Monte Carlo simulations of the kinetics of domain growth for weakly incommensurate phases, and second, the structure for  $T < T_c$  is unknown experimentally for  $\text{AlCl}_3$ -GICs. Therefore we suggest that the time evolution of the CCSR linewidth observed near  $T_c$  can be attributed to the time growing of the average linear domain size of unknown yet, probably a weak incommensurate triangular superlattice with high  $Q$  degeneracy,  $Q > 10$ , (21). At lower temperatures ( $T < 140K$ ) the observation of a slower ordering kinetics could be due either to a configuration of frozen-in microdomains forming a quasi-2D glasslike state, or (unlikely) to pinning effects due to square or honeycomb superlattices.

The sluggish kinetics observed after an elapsed time of 40 minutes near the transition temperature,  $n = 0.32 \pm 0.06$  (see fig.5), can be attributed to a pinning of the domain boundaries on the Daumas-Herold domain walls. Our data does not reveal any effect of critical fluctuations near the transition temperature (25).

#### CONCLUSIONS

In this work we showed that CCSR can give valuable information about the charge transport properties in GICs. Also we believe that the observed time broadening of the CCSR linewidth could be attributed to the time growing of the average domain size of, probably, a weak incommensurate superlattice. Then, we showed that CCSR experiment can be a very helpful technique for studying the

kinetics of quasi-2D domain ordering in GICs.

This work was partially supported by FAPESP and CNPq, Brazil.

27, 1085 (1979).

24. S.A.Safran, Phys.Rev.Lett 46, 1581 (1981).

25. S.A.Safran, P.S.Sahni and G.Grest, Phys.Rev.B28, 2693 (1983).

#### REFERENCES

1. K.A.Muller and R.Kleiner, Phys.Lett. 1, 98 (1982).
2. G.Wagoner, Phys.Rev. 118, 647 (1960).
3. P.Lauginie, H.Estrade J.Conard D. Guérard, P.Lagrange and M.El Makrini 99B, 514 (1980)
4. M.Murata and H.Suematsu, J.Phys.Soc.Jpn 51, 1337 (1982).
5. S.K.Khanna, E.R.Falardeau, A.J. Heeger, and J.E.Fischer, Sol.Stat.Comm. 25, 1059 (1978)
6. A.Baiker, E.Habegger, V.K.Sharma, and W.Richarz, Carbon 19, 327 (1981)
7. R.M.Stein, L.Walsmley, G.M.Gualberto and C.Rettori, Phys.Rev.B32, 4774 (1985).
8. G.M.Gualberto, C.Underhill, S.Y. Leung and G.Dresselhaus, Phys.Rev.B21 862(1980).
9. L.Walsmley, S.Rolla, and C.Rettori to be published.
10. F.J.Dyson, Phys.Rev. 98, 349 (1955).
11. G.Feher and A.F.Kip, Phys.Rev. 98 337 (1956).
12. C.Zeller, L.A.Pendrys, and F.L.Vogel J.Mater.Sci.14, 2241 (1979).
13. J.F.Mareche E.Mc Rae, N.Nodi, R. Vangelisti, Synth. Met. 8, 163 (1983).
14. L.Pietronero and S.Strassler, Synth Met. 3, 213 (1981).
15. M.S.Dresselhaus, G.Dresselhaus, Adv. Phys. 30, 139 (1981).
16. D.T.Morelli and C.Uher, Phys.Rev. B27, 2477 (1983).
17. R.J.Elliot, Phys.Rev. 96, 266 (1954)
18. H.Homma and R.Clarke, Phys.Rev. B31 5865 (1985).
19. D.M.Huang and G.Nicolaides, Sol.Stat. Comm., 49 483 (1984).
20. D.M.Bittner and M.Bretz, Phys.Rev. B31, 1060 (1985).
21. P.S.Sahni, D.J.Srolovitz G.S.Grest M.P.Anderson and S.A.Safran, Phys.Rev. B28, 2705 (1983).
22. M.Lifshitz, Zh.Eksp.Teor.Fiz. 42 354 (1962) / Sov.Phys. JETP 15 939 (1962).
23. S.M.Allen and J.W.Cahn, Acta Metali